The International Journal of Advanced Manufacturing Technology (2022) 123:4293–4308
https://doi.org/10.1007/s00170-022-10430-w

ORIGINAL ARTICLE

A machine learning approach for ball milling of alumina ceramics

Jungwon Yu[1] · Kati Raju[2] · So-Hyun Jin[2] · Youngjae Lee[1] · Hyun-Kwuon Lee[2]

Received: 22 May 2022 / Accepted: 2 November 2022 / Published online: 19 November 2022

Abstract
In this work, machine learning approach based on polynomial regression was explored to analyze the optimal processing parameters and predict the target particle sizes for ball milling of alumina ceramics. Data points were experimentally collected by measuring the particle sizes. Prediction interval (PI)-based optimization methods using polynomial regression analysis are proposed. As a first step, functional relations between processing parameters (inputs) and quality responses (outputs) are derived by applying the regression analysis. Later, based on these relations, objective functions to be maximized are defined by desirability approach. Finally, the proposed PI-based methods optimize both parameter points and intervals of the target mill for accomplishing user-specified target responses. The optimization results show that the PI-based point optimization methods can select and recommend statistically reliable optimized parameter points even though unique solutions for the objective functions do not exist. From the results of confirmation experiments, it is established that the optimized parameter points can produce desired final powders with quality responses quite similar to the target responses.

Keywords Alumina · Wet ball mill · Machine learning · Polynomial regression analysis · Prediction interval · Parameter optimization

1 Introduction

Machine learning (ML) methods have accelerated the scientific advancement in recent times since they are capable of analyzing of large amounts of data (big data), and thus, they can select the optimal processing parameters more precisely. Due to their longer cycles and low efficiencies, traditional methods, such as the empirical trial and error methods, are unable to keep pace with the development of material analysis and design. Accordingly, due to their low computational costs and short development cycles, ML methods coupled with powerful data processing and high prediction performance are widely used. ML methods have been successfully applied in various fields including glasses [1–5], ceramics [6, 7], biomaterials [8], and material science [1, 4, 9, 10] for the prediction of various mechanical properties, kinetic properties, thermal resistance properties, and many more. These ML methods demonstrated their efficacy by the way the input data is processed and analyzed quantitatively. ML methods are successfully applied for the discovery of high-entropy ceramics [11] and alloys [12]. And also, for the prediction of permittivity for microwave dielectric ceramics [13], the melting temperature of ultra-high temperature ceramics [14], and the bending strength of silicon nitride ceramics [15].

Reliable, robust, and accurate experimental input data is essential for ML since many methods are based on supervised learning approaches, in which the models are trained properly through the input data. It is also possible to predict the target values with a great accuracy through these ML methods, and therefore, selection of appropriate method is very important. Regression models are capable of predicting continuous outputs and are generally trained by minimizing a squared error loss function of a training data set. Regression-based ML methods have been applied efficaciously on different materials for the optimization and prediction of various properties [2, 3, 6–8]. For instance, Yang et al. [2] predicted the Young's modulus of silicate glasses by combining ML with high-throughput molecular

✉ Hyun-Kwuon Lee
hklee@kumoh.ac.kr

[1] Electronics and Telecommunications Research Institute, Daegu-Gyeongbuk Research Center, Daegu 42994, South Korea

[2] School of Advanced Materials Science and Engineering, Kumoh National Institute of Technology, Gumi, Gyeongbuk 39177, South Korea

dynamics. The dissolution kinetics of silicate glasses by topology-informed ML was predicted by Liu et al. [3]. And, interfacial thermal resistance between graphene and hexagonal boron nitride was predicted by Yang et al. by artificial neural network (ANN) models [6]. However, ML methods have been applied very rarely to address the issues in the field of ceramics ball milling.

Ball mill is one of the most popular comminution machines used to produce desired reduced particle sizes and particle size distributions (PSDs) of starting powders [16–18]. It has been widely applied for fine grinding of materials in various fields including ceramics, mineral processing, and electronics. Ball milling in general and wet ball milling in particular is a complex process governed by various processing parameters such as slurry amounts [19], powder and ball loadings [20], milling speeds and times [21, 22], container and ball sizes [23], and so on; the quality of produced powders also depends on the types and properties of starting powders. Therefore, optimizing these processing parameters is absolutely needed in ceramics processing to achieve user-specified target values.

Many of present-day industrial applications demand comprehensive theoretical simulations before experimental design. Therefore, for the optimization of engineering manufacturing processes, statistical experiment design techniques (e.g., Taguchi method and response surface method (RSM)) and computer modeling techniques such as ANN and genetic algorithms (GA) have been used. Numerous studies have been made to optimize input parameters of ball milling processes for different materials including TiO_2 [24], WC–Co [25], WC–MgO [26], zeolite [27], calcite [28], refractory ores [29, 30], and Al 2024 alloy powders [31]. Hou et al. [24] integrated the parameter design of the Taguchi method, RSM and GA and applied to optimize the milling process parameters for titania nanoparticles. Patil and Anandhan [32] employed Taguchi method to analyse the effect of planetary milling of fly ash and analysis of variance (AVOVA) was used to decide the effect of significance of input parameters. Central composite design (CCD), a standard RSM designed experiment, was implemented by Erdemir [33] to determine the effects of high energy milling parameters for micro and nano boron carbide powders. The adequacy of mathematical models and the significance of the regression coefficients were analyzed using ANOVA. Petrovic et al. [34] optimized the ball milling parameters for TiO_2–CeO_2 nano powders through RSM by utilising CCD. Regression analysis showed good agreement of experimental data with second-order polynomial model. Taguchi methodology was used by Hajji et al. [35] for the mechanosynthesis of hydroxyfluorapatite using planetary ball milling. Recently, Santosh et al. [36] optimized the mill parameters by carrying out systematic design experiments on the selected low-grade chromite ore. For this purpose, stirrer speed, grinding time, feed size, and solids concentration were varied as per CCD design. However, these studies have several limitations; for instance, most studies focused on optimizing milling parameters using only one quality response (mostly median particle size, d_{50}). If, in addition to the d_{50}, the shape of PSDs is also considered as quality responses, multiple response optimization (MRO) problems should be dealt with. The methods based on the main effect plots cannot handle the MRO problems in which the trade-off between multiple responses should be treated. And also, most studies had little regard to solve such optimization problems in ball milling that desired target values for quality responses are set up. Main effect plots can maximize or minimize quality responses but cannot minimize the differences between the response values and their target values. Moreover, very few studies have attempted to optimize both milling parameter points and their intervals. The optimized parameter intervals can help to operate the target mill more flexibly by considering process uncertainties caused by measurement errors for quality responses, setting errors of processing parameters, and errors occurred by omitting uncontrollable factors (e.g., temperature and humidity).

This paper proposes prediction interval (PI)-based optimization methods for optimizing a wet ball mill using polynomial regression analysis. The aim of the proposed methods is to optimize both parameter points and intervals of the target mill by solving such MRO problems that user-specified target values are set up for some quality responses. After deriving the regression functions from the collected dataset and defining objective functions, the proposed PI-based optimization methods were applied for optimizing both parameter points and intervals of the target mill. To verify the effectiveness of the optimized parameter points, confirmation experiments were also performed several times. Herein, we report on the applicability of polynomial regression-based ML approach for ball milling of alumina ceramics. Experimental data points were collected systematically via particle size analysis. Using this model, the optimal processing parameters can be selected and the response values can be predicted based on the values of processing parameters. In particular, a quantitative analysis of the factors affecting the particle size was conducted. Although this study focuses on the ball milling of alumina ceramics, the proposed new approach reported could be applied for other ceramic materials as well.

2 Experimental details

The five processing parameters (inputs) and the three quality responses (outputs) of the target mill are summarized in Table 1. Al_2O_3 powders (AES-11, purity of 99.9%, $d_{50}=0.7$ μm, $d_{90}=1.96$ μm, Sumitomo Chemical, Japan)

Table 1 Five processing parameters x_1,…, x_5 and three quality responses y_1,…, y_3 of target mill

Symbol	Variable
x_1	Volume percent of slurry (vol%)
x_2	Solid content (wt%)
x_3	Milling speed (%)
x_4	Milling time (hour)
x_5	Ball size (mm)
y_1	Median particle size (d_{50})
y_2	Width of PSD
y_3	Skewness of PSD

preliminary and optimization phases. In the preliminary phase, first, functional relations $\hat{y}_l(\mathbf{x})$, $l=1,\ldots, L$, between p inputs (i.e., processing parameters) and L outputs (i.e., quality responses) are derived by applying the regression analysis to an experimental dataset $\{(\mathbf{x}_i \in \Re^p; \mathbf{y}_i \in \Re^L)\}_{i=1}^n$. Second, based on the $\hat{y}_l(\mathbf{x})$, importance values of p inputs for each output are estimated by Monte Carlo (MC)-based method; the importance matrix $\mathbf{I}_{imp.} \in \Re^{L\times p}$ that consists of the estimated importance values can be employed to prioritize processing parameters and to optimize parameter intervals. Third, objective functions $D(\mathbf{x})$ to be maximized for solving MRO problems are defined by desirability approach. In the optimization phase, first, the proposed point optimization method is applied to $D(\mathbf{x})$ for obtaining K' optimized parameter points $\{\mathbf{x}^*_{(1)}, \ldots, \mathbf{x}^*_{(K')}\}$ to be recommended for the users (e.g., process operators and engineers). After that, the proposed interval optimization method is used to find upper and lower bound vectors $\mathbf{x}^*_{LB} = [x^*_{LB,1}, \ldots, x^*_{LB,p}]^T$ and $\mathbf{x}^*_{UB} = [x^*_{UB,1}, \ldots, x^*_{UB,p}]^T$ that can define parameter intervals $[x^*_{LB,j}, x^*_{UB,j}]$, $j=1,\ldots, p$, enclosing an optimized point $\mathbf{x}^* \in \{\mathbf{x}^*_{(1)}, \ldots, \mathbf{x}^*_{(K')}\}$.

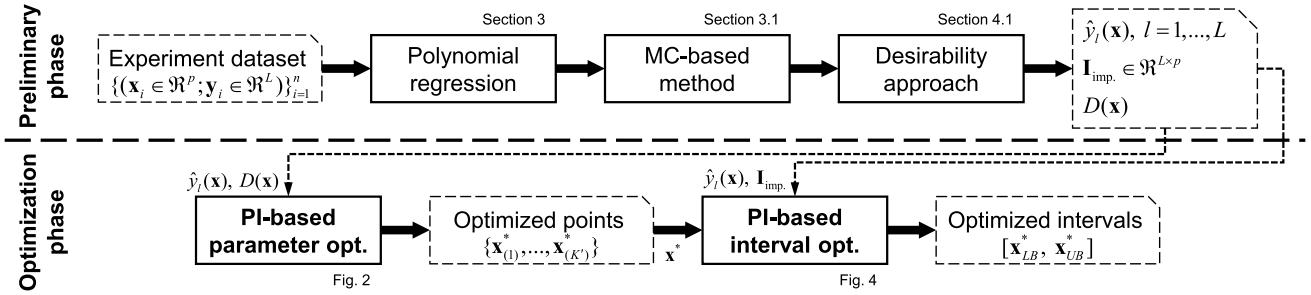

Fig. 1 Procedure for the proposed PI-based optimization methods for optimizing parameter points and intervals

were used as starting powders. The value of d_{50} (y_1), and the values of width and skewness (y_2 and y_3) reflecting the shape of PSDs are employed as quality responses to assess milled alumina powders. The volume percent of slurry (x_1), solid content (x_2), milling speed (x_3), milling time (x_4), and ball size (x_5) are considered as key processing parameters affecting these responses. In this paper, the proposed PI-based optimization methods are applied to the same experiment dataset used in our recent publication [37]. Except for the milling time (x_4) and the ball size (x_5), the ranges and levels of the x_1, x_2, and x_3 were set up, and fifteen times milling experiments were designed by CCD. The same set of the milling experiments (i.e., the fifteen times experiments) was repeated with three different ball sizes (i.e., 3, 5, and 10 mm); the total number of conducted experiments were 45 ($=15\times3$). At each experiment, milling was carried out for 24 h, and after 4, 8, 12, and 24 h from the start of milling, the values of the quality responses were measured and calculated. The total of 180 ($=45\times4$) data pairs were prepared, each of which consists of the setting values of the five milling parameters (inputs) and the measured values of the three responses (outputs) (see supplementary information). More experimental details about the ball milling and processing parameters can be found elsewhere [37].

Figure 1 summarizes the procedure for the proposed PI-based optimization methods, which is roughly divided into

3 Polynomial regression analysis

Second-order polynomial regression analysis [29, 38–40] has been popularly used to optimize processing parameters in various industrial fields including powder processing using ball milling, since it can construct highly interpretable regression models that can appropriately capture the nonlinearities contained in such experimental datasets with relatively low model complexity. For example, RSM was employed by Costa and Garcia [41] to optimize the efficiency of a refrigeration cycle demonstration using MRO approach. Mostafanezhad et al. [42] analysed the formability of aluminium in two-point incremental forming process by employing RSM. Parida et al. [43] employed RSM with full

factorial design for the modelling and analysing the response parameters in the case of reduction of emissions in a variable compression ratio engine. RSM based quadratic models have been established between the parameters and proposed characteristics by Yaliwal et al. [44] in the case of biodiesel-producer gas operated compression ignition engine.

Functional relations between p inputs $x_1,\ldots, x_p$ and lth output y_l ($l=1,\ldots, L$) are formulated by the regression analysis as follows [37]:

$$y_l = f_l(\mathbf{x}|\boldsymbol{\beta}^l) + \varepsilon_l = \beta_0^l + \sum_{j=1}^{p} \beta_j^l x_j + \sum_{j<k} \beta_{jk}^l x_j x_k + \sum_{j=1}^{p} \beta_{jj}^l x_j^2 + \varepsilon_l \tag{1}$$

where ε_l is an error term, β_0^l is an intercept, and β_j^l, β_{jk}^l, and β_{jj}^l are regression coefficients associated with linear, interaction, and quadratic terms, respectively. In Eq. (1), the total number of coefficients to be estimated is $p' = 1 + 2p + p(p-1)/2$. Let $\mathbf{y}_l = [y_{1l},\ldots, y_{nl}]^T \in \mathfrak{R}^n$ and $\mathbf{Z} = [\mathbf{z}_1,\ldots, \mathbf{z}_n]^T \in \mathfrak{R}^{n\times p'}$ be the output vector that consists of n observations for lth output and the design matrix, respectively; the ith row of $\mathbf{Z}$ is $\mathbf{z}_i^T = \mathbf{z}(\mathbf{x}_i)^T = [1, x_{i1},\ldots, x_{ip}, x_{i1}x_{i2},\ldots, x_{i(p-1)}x_{ip},\ldots, x_{i1}^2,\ldots, x_{ip}^2]$, where $\mathbf{z}(\cdot): \mathfrak{R}^p \to \mathfrak{R}^{p'}$. Without loss of generality, it can be assumed that the values of all inputs $x_1,\ldots, x_p$ have been standardized to be in the range $[-1, 1]$. The coefficient vector $\boldsymbol{\beta}^l \in \mathfrak{R}^{p'}$ composed of the p' coefficients can be estimated by the method of least squares as follows: $\hat{\boldsymbol{\beta}}^l = (\mathbf{Z}^T\mathbf{Z})^{-1}\mathbf{Z}^T\mathbf{y}_l$. An unbiased estimator for the standard deviation σ_{ε_l} of the ε_l is $s_l = \sqrt{\frac{1}{n-p'}\sum_{i=1}^{n}(y_{il} - \hat{y}_{il})^2}$, where $\hat{y}_{il} = \mathbf{z}_i^T\hat{\boldsymbol{\beta}}^l$, $i=1,\ldots, n$. The standard error (SE) of the j'th component $\hat{\beta}_{j'}^l$ in $\hat{\boldsymbol{\beta}}^l$ is $SE(\hat{\beta}_{j'}^l) = s_l\sqrt{(\mathbf{Z}^T\mathbf{Z})_{j'j'}^{-1}}$, $j'=1,\ldots, p'$, where $(\mathbf{Z}^T\mathbf{Z})_{j'j'}^{-1}$ is the j'th diagonal element of the matrix $(\mathbf{Z}^T\mathbf{Z})^{-1}$. The t-statistic used to test the statistical significance of the j'th term in the vector $\mathbf{z} \in \mathfrak{R}^{p'}$ is calculated as $t_{j'}^l = \hat{\beta}_{j'}^l \Big/ SE(\hat{\beta}_{j'}^l)$, and it follows the t-distribution $t(n-p')$ with degree of freedom $n-p'$. The p value of $t_{j'}^l$ is defined as $\Pr(|T| > t_{j'}^l)$, where $T \sim t(n-p')$; the lower the p value, the higher the statistical significance of the j'th term in $\mathbf{z}$. In this paper, the terms with p values smaller than 0.1 are regarded to be statistically significant.

The output of the lth regression function in Eq. (1) for a new input vector $\mathbf{x}_{\text{new}} = [x_{\text{new},1},\ldots, x_{\text{new},p}]^T$ can be calculated as $\hat{y}_l(\mathbf{x}_{\text{new}}) = \mathbf{z}(\mathbf{x}_{\text{new}})^T\hat{\boldsymbol{\beta}}^l = \mathbf{z}_{\text{new}}^T\hat{\boldsymbol{\beta}}^l$, and its $100(1-\alpha)\%$ PI, $[PI_{LB}^l(\mathbf{x}_{\text{new}}), PI_{UB}^l(\mathbf{x}_{\text{new}})]$, is calculated as

$$\begin{aligned} PI_{LB}^l(\mathbf{x}_{\text{new}}) &= \hat{y}_l(\mathbf{x}_{\text{new}}) - t_{1-\alpha/2}(n-p')s_l\sqrt{1 + \mathbf{z}_{\text{new}}^T(\mathbf{Z}^T\mathbf{Z})^{-1}\mathbf{z}_{\text{new}}} \\ PI_{UB}^l(\mathbf{x}_{\text{new}}) &= \hat{y}_l(\mathbf{x}_{\text{new}}) + t_{1-\alpha/2}(n-p')s_l\sqrt{1 + \mathbf{z}_{\text{new}}^T(\mathbf{Z}^T\mathbf{Z})^{-1}\mathbf{z}_{\text{new}}} \end{aligned} \tag{2}$$

where α is significance level for PI, and $t_{1-\alpha/2}(n-p')$ is the $1-\alpha/2$ percentile of the t distribution $t(n-p')$.

3.1 MC-based method for estimating importance values of inputs

In this work, the following Monte Carlo (MC)-based method is used to estimate importance values of p inputs x_j ($j=1,\ldots, p$) for the lth output y_l ($l=1,\ldots, L$); this is a modified version of the method presented in [45, 46]. First of all, after generating N uniform random vectors $\mathbf{x}^{(1)},\ldots, \mathbf{x}^{(N)}$ with p dimensions, these vectors are substituted into the lth regression function $\hat{y}_l(\mathbf{x}) = f_l(\mathbf{x}|\hat{\boldsymbol{\beta}}^l)$ to obtain N output values $y_l^{(1)},\ldots, y_l^{(N)}$, and their median $y_{l,\text{med}}$ is calculated. The random vectors can be partitioned into two sets as follows: $X_{\text{larger}}^l = \{\mathbf{x}^{(i)} | \hat{y}_l^{(i)} \geq y_{l,\text{med}},\ i = 1,\ldots, N\}$ and $X_{\text{smaller}}^l = \{\mathbf{x}^{(1)},\ldots, \mathbf{x}^{(N)}\} \backslash X_{\text{larger}}^l$. And then, two empirical cumulative distribution functions (ECDFs), $F_{\text{larger}}^l(x_j)$ and $F_{\text{smaller}}^l(x_j)$ for each input x_j are estimated based on the jth elements of the vectors in X_{larger}^l and X_{smaller}^l, respectively. In [45, 46], Kolmogorov Smirnov distance between $F_{\text{larger}}^l(x_j)$ and $F_{\text{smaller}}^l(x_j)$ was regarded as the importance value of the jth input x_j for the lth response y_l. In this paper, to estimate the importance value more precisely, the total area of the region(s) surrounded by the two ECDFs are calculated by numerical integration. Finally, the calculated total area is regarded as the importance value of x_j for y_l. Finishing the above procedure, importance matrix $\mathbf{I}_{\text{imp.}} \in \mathfrak{R}^{L\times p}$ composed of the estimated importance values is returned.

4 Optimization of parameter points and intervals

4.1 Desirability approach

Desirability approach [47–49] has been commonly employed for defining objective functions for MRO problems in which multiple quality responses with different ranges are handled. Depending on whether a response y_l should be minimized, maximized, or as close as possible to a target value $y_{l,\text{target}}$, different desirability functions are used, and these functions transform the output value $\hat{y}_l(\mathbf{x})$ to have the range of 0 to 1. If there are user-specified target values for y_l, the following is used as its desirability function:

$$d_l\left(\hat{y}_l(\mathbf{x})\right) = \begin{cases} 0 & \text{if } \hat{y}_l(\mathbf{x}) < y_{l,\min} \\ \left(\frac{\hat{y}_l(\mathbf{x}) - y_{l,\min}}{y_{l,\text{target}} - y_{l,\min}}\right)^s & \text{if } y_{l,\min} \leq \hat{y}_l(\mathbf{x}) \leq y_{l,\text{target}} \\ \left(\frac{\hat{y}_l(\mathbf{x}) - y_{l,\max}}{y_{l,\text{target}} - y_{l,\max}}\right)^t & \text{if } y_{l,\text{target}} \leq \hat{y}_l(\mathbf{x}) \leq y_{l,\max} \\ 0 & \text{if } \hat{y}_l(\mathbf{x}) > y_{l,\max} \end{cases} \tag{3}$$

where $y_{l,\min}$ and $y_{l,\max}$ are the lower and upper limits of y_l, respectively, both of which can be obtained from the observations $y_{1l},\ldots, y_{nl}$; $y_{l,\text{target}} \in [y_{l,\min}, y_{l,\max}]$ is a target value for

y_l, and s and t are design values that determine the shape of Eq. (3). If the lth response should be minimized, the following desirability function is used:

$$d_l\left(\hat{y}_l(\mathbf{x})\right) = \begin{cases} 1 & \text{if } \hat{y}_l(\mathbf{x}) < y_{l,\min} \\ \left(\dfrac{y_{l,\max} - \hat{y}_l(\mathbf{x})}{y_{l,\max} - y_{l,\min}}\right)^t & \text{if } y_{l,\min} \le \hat{y}_l(\mathbf{x}) \le y_{l,\max} \\ 0 & \text{if } \hat{y}_l(\mathbf{x}) > y_{l,\max} \end{cases} \tag{4}$$

The desirability function used when the response should be maximized is similar to Eq. (4), and thus omitted due to space constraints. In this paper, both design values of s and t in Eqs. (3) and (4) are set to 1.

The following overall desirability function $D(\mathbf{x})$, a weighted geometric mean of $d_l(\bullet)$, $l = 1,\ldots, L$, is used as objective functions for MRO problems:

$$D(\mathbf{x}) = \left(\prod_{l=1}^{L} d_l\left(\hat{y}_l(\mathbf{x})\right)^{w_l}\right)^{1/\sum_l w_l} \tag{5}$$

where w_l is a weight value assigned to lth response; in this paper, all weight values are set to 1. Depending on the priority of quality responses, their weight values can be differently set up. For example, if making the value of d_{50} (y_1) to be closer to its target value is more preferable than minimizing the value of width (y_2), the value of w_1 should be set to be larger than the value of w_2 (e.g., $w_1 = 5$ and $w_2 = 1$).

4.2 PI-based method for optimizing parameter points

It should be noted that unique solutions do not exist in such MRO problems that some quality responses want to be equal to user-specified target values. That is, whenever executing optimization algorithms (e.g., quadratic programming and particle swarm optimization (PSO)) to maximize $D(\mathbf{x})$, different solutions are discovered each time. It is, therefore, essential to decide which of these different solutions to be selected and then recommended for users. Among these different solutions, the proposed PI-based point optimization method (Fig. 2) selects statistically significant solutions (i.e., optimized parameter points) based on the lengths of their PIs. Here, it is assumed that as the length of PIs for a solution becomes shorter, its uncertainty is reduced from a statistical viewpoint. The proposed method is an advanced version of the method in [50] so that it can be also applicable for MRO problems, and the quality of the different solutions is quantified in terms of PIs instead of confidence intervals. PIs for optimized parameter points need to be calculated beforehand to optimize their parameter intervals, as will be described in Section 5, PIs are also helpful to interpret the

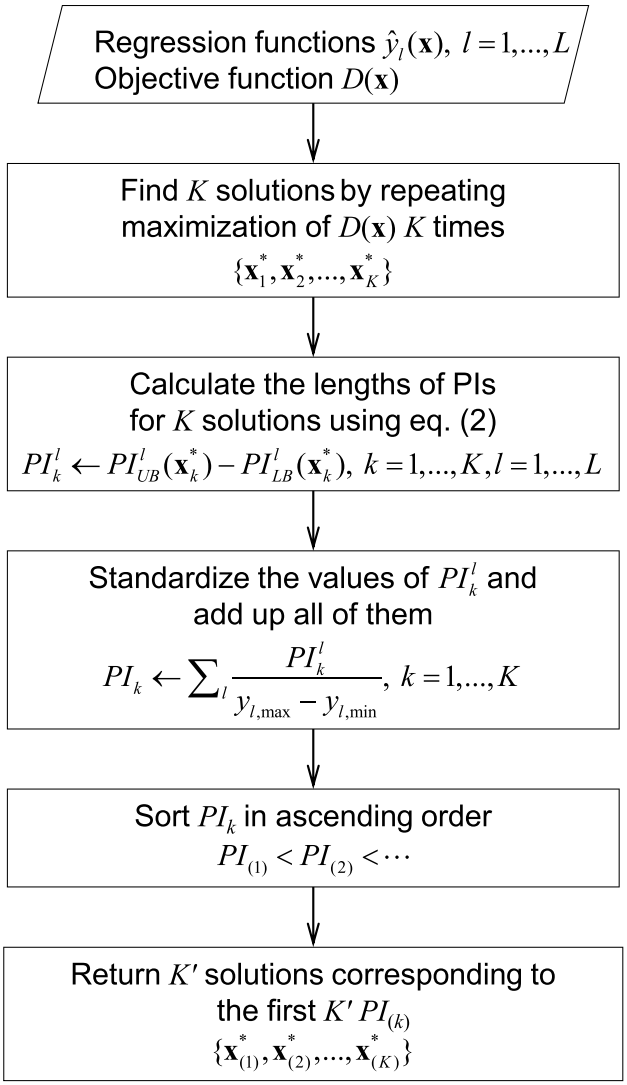

Fig. 2 Flowchart of the proposed PI-based method for optimizing parameter points

prediction results of quality responses and the results of confirmation experiments.

In the proposed method in Fig. 2, firstly, K different solutions $\mathbf{x}_k^*$, $k = 1,\ldots, K$, are obtained by applying an optimization algorithm to maximize $D(\mathbf{x})$ K times. To do this, any optimization algorithm (derivative-based or derivative-free) can be employed. In this work, PSO [51–53], a well-known global optimization algorithm, was applied to find these solutions; the 'particleswarm' MATLAB function built into Global Optimization Toolbox can be used to maximize $D(\mathbf{x})$. The detailed explanations for PSO algorithm are redundant, so they are omitted due to space constraints; for more details of PSO, readers are invited to see Refs. [51–53]. After finding the K solutions, the lengths of L PIs, $PI_k^l = PI_{UB}^l(\mathbf{x}_k^*) - PI_{LB}^l(\mathbf{x}_k^*)$, $l = 1,\ldots, L$, for all k are calculated using Eq. (2); the upper and lower limits $y_{l,\max}$ and $y_{l,\min}$ of y_l are used to

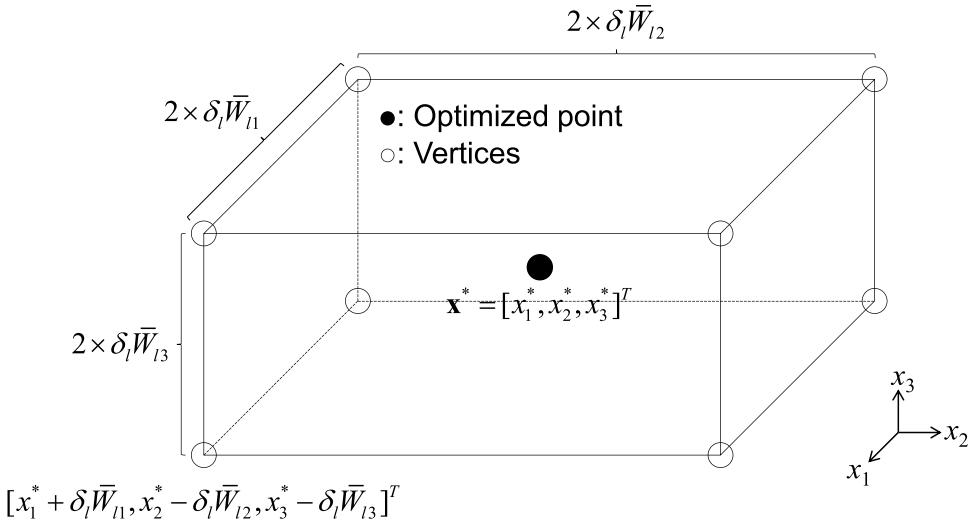

Fig. 3 Example of the hyper-rectangle defined in a three-dimensional input space

standardize the values of PI_k^l. Finally, PI_k, $k=1,\ldots, K$, obtained by summing all the standardized values of PI_k^l, are sorted in ascending order (i.e., $PI_{(1)}<PI_{(2)}<\cdots$), and then the K' solutions $\mathbf{x}_{(1)}^*,\ldots,\mathbf{x}_{(K')}^*$ relevant with the first K' PI_k are returned.

4.3 PI-based method for optimizing parameter intervals

To deal with the process uncertainties, in addition to an optimized parameter point $\mathbf{x}^*=[x_1^*,\ldots,x_p^*]^T$, it is also necessary to obtain statistically meaningful optimized parameter intervals $[x_{LB,j}^*, x_{UB,j}^*]$, $j=1,\ldots, p$, enclosing the point $\mathbf{x}^*$, i.e.,$x_j^* \in[x_{LB,j}^*, x_{UB,j}^*]$, $\forall j$. It is desirable that parameter points belonging to the input domain restricted by these p intervals can achieve similar quality responses with those of $\mathbf{x}^*$.

In the p-dimensional input space, an hyper-rectangle (i.e., orthotope) that is centered at $\mathbf{x}^*$ and has 2^p vertices $\mathbf{v}_m\in\Re^p$, $m=1,\ldots, 2^p$, can be imagined. Figure 3 shows the example of the hyper-rectangle with 8 ($=2^3$) vertices defined in a three-dimensional input space. For each l, while redefining the hyper-rectangle by increasing the length of its edges gradually, one can discover the one defined immediately before any of output values $\hat{y}_l(\mathbf{v}_m)$ of all the 2^p vertices start to depart from the PIs of $\mathbf{x}^*[PI_{LB}^l(\mathbf{x}^*),PI_{UB}^l(\mathbf{x}^*)]$. The parameter intervals can be easily obtained from the L discovered hyper-rectangles. Weight values $\overline{W}_{lj}(j=1,\ldots, p, l=1,\ldots, L)$ calculated from the importance matrix $\mathbf{I}_{\text{imp.}}$ can be used to differentially increase the length of edges according to the importance values; the larger the importance value of x_j, the shorter the length of the edges in parallel with the jth input direction.

In the proposed PI-based interval optimization method, for each l, the hyper-rectangle in which the length of the edges in parallel with the jth input direction is $2\times\delta_l\overline{W}_{lj}$ are firstly defined, where $\delta_l>0$ is a small positive increment; this can be represented as a Cartesian product of p intervals as follows [54]:$\times_{j=1}^p[x_j^*-\delta_l\overline{W}_{lj}, x_j^*+\delta_l\overline{W}_{lj}]$, where $\times$ is the Cartesian product operator. Second, the 2^p vertices are organized into the vertex set $V=\{\mathbf{v}_m\in\Re^p|m=1,\ldots, 2^p\}$. While increasing the length of the edges, the elements of $\mathbf{v}_m$ that become larger than $+1$ (or smaller than -1) are replaced by $+1$ (or -1). The reason for this is that each element of input vector $\mathbf{x}$ in the regression functions $\hat{y}_l(\mathbf{x})$ must be located in the range $[-1, 1]$. Third, the maximum value of δ_l that makes the outputs $\hat{y}_l(\mathbf{v}_m)$ of all $\mathbf{v}_m$ to be included in the lth PI $[PI_{LB}^l(\mathbf{x}^*), PI_{UB}^l(\mathbf{x}^*)]$ is found by slightly increasing the value of δ_l. Fourth, after finding the maximum values of δ_l,$\delta_l^{\max}$, for all l, the following upper and lower bound vectors $\mathbf{x}_{UB}^l$ and $\mathbf{x}_{LB}^l$, are defined:

$$\begin{aligned}\mathbf{x}_{UB}^l &= [x_1^*+\delta_l^{\max}\overline{W}_{l1},\ldots,x_p^*+\delta_l^{\max}\overline{W}_{lp}]^T \text{ and } \mathbf{x}_{LB}^l\\ &= [x_1^*-\delta_l^{\max}\overline{W}_{l1},\ldots,x_p^*-\delta_l^{\max}\overline{W}_{lp}]^T\end{aligned} \tag{6}$$

In Eq. (6), all the components of $\mathbf{x}_{UB}^l$ and $\mathbf{x}_{LB}^l$ larger than $+1$ (or smaller than -1) must be replaced by $+1$ (or -1). Based on $\mathbf{x}_{UB}^l$ and $\mathbf{x}_{LB}^l$, $l=1,\ldots, L$, the L different hyper-rectangles can be defined as:$\times_{j=1}^p[x_{LB,j}^l, x_{UB,j}^l]$, $l=1,\ldots, L$. It is important to note that the L regions occupied by these L hyper-rectangles can be different from each other. Finally, the upper and lower bound vectors that can define the overlap between all the L hyper-rectangles are obtained as follows:

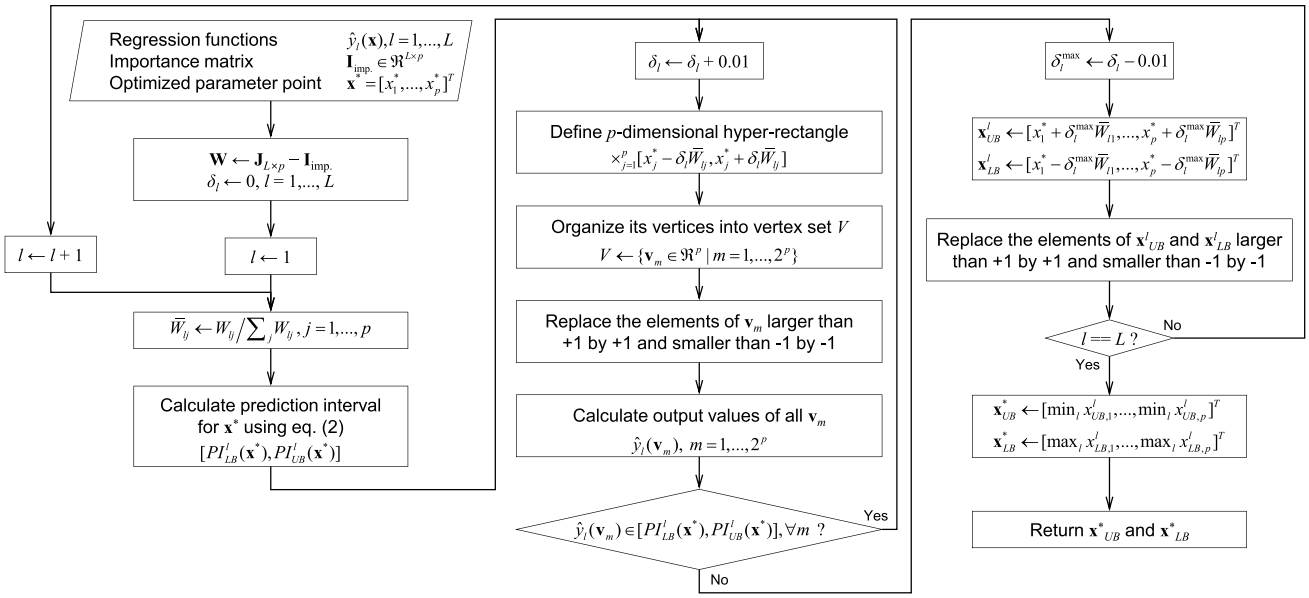

Fig. 4 Flowchart of the proposed PI-based method for optimizing parameter intervals

Table 2 Performance indices of full and reduced models for three responses

Performance index	$\hat{y}_1(\mathbf{x})$		$\hat{y}_2(\mathbf{x})$		$\hat{y}_3(\mathbf{x})$	
	Full	Reduced	Full	Reduced	Full	Reduced
RMSE	0.0131	0.0131	0.135	0.134	0.0205	0.0202
R^2	0.753	0.742	0.759	0.747	0.867	0.864
Adjusted R^2	0.722	0.722	0.729	0.733	0.851	0.855
F-statistic	24.3	36.7	25	55.7	51.9	97.1

$$\mathbf{x}_{UB}^* = [\min_l x_{UB,1}^l, ..., \min_l x_{UB,p}^l]^T \text{and } \mathbf{x}_{LB}^* = [\max_l x_{LB,1}^l, ..., \max_l x_{LB,p}^l]^T \quad (7)$$

The vectors $\mathbf{x}_{UB}^*$ and $\mathbf{x}_{LB}^*$ consist of the upper and lower bounds of the optimized parameter intervals $[x_{LB,j}^*, x_{UB,j}^*]$, $j=1,\ldots,p$, for $\mathbf{x}^*$, respectively. The statistically meaningful optimized parameter intervals $[x_{LB,j}^*, x_{UB,j}^*]$ can define the region of input space that contains the input points satisfied with the following property: the output values $\hat{y}_l(\mathbf{x})$ of all points in the region are included in the PI $[PI_{LB}^l(\mathbf{x}^*), PI_{UB}^l(\mathbf{x}^*)]$ of the optimized parameter point $\mathbf{x}^*$. In other words, the points included in the region defined by the optimized intervals can obtain statistically similar quality responses with those of the point $\mathbf{x}^*$. Owing to this property of the optimized intervals, fine-tuning the point $\mathbf{x}^*$ within the region can be permissible. The proposed PI-based interval optimization method explained so far is summarized in Fig. 4.

5 Results and discussion

5.1 Results of regression analysis

To derive regression functions between $p=5$ inputs and $L=3$ outputs, three full models in Eq. (1) with $p'=21$ regression coefficients are fitted to the 180 data pairs via the method of least squares; all the input values should be standardized to belong in the range $[-1, 1]$ in advance. Since the number of data samples are limited, instead of splitting them into training and validation sets, entire samples are employed to build regression models. To validate their generalization abilities, the performance indices in Table 2 will be closely examined. In the full models, the order of polynomial (i.e., hyperparameter) is set to 2; as described in Section 3, the collected dataset by CCD can be thoroughly explained by these models. Although not presented in this paper due to space constraints, the results of explanatory data analysis via scatter plots and main effect plots also indicated that it

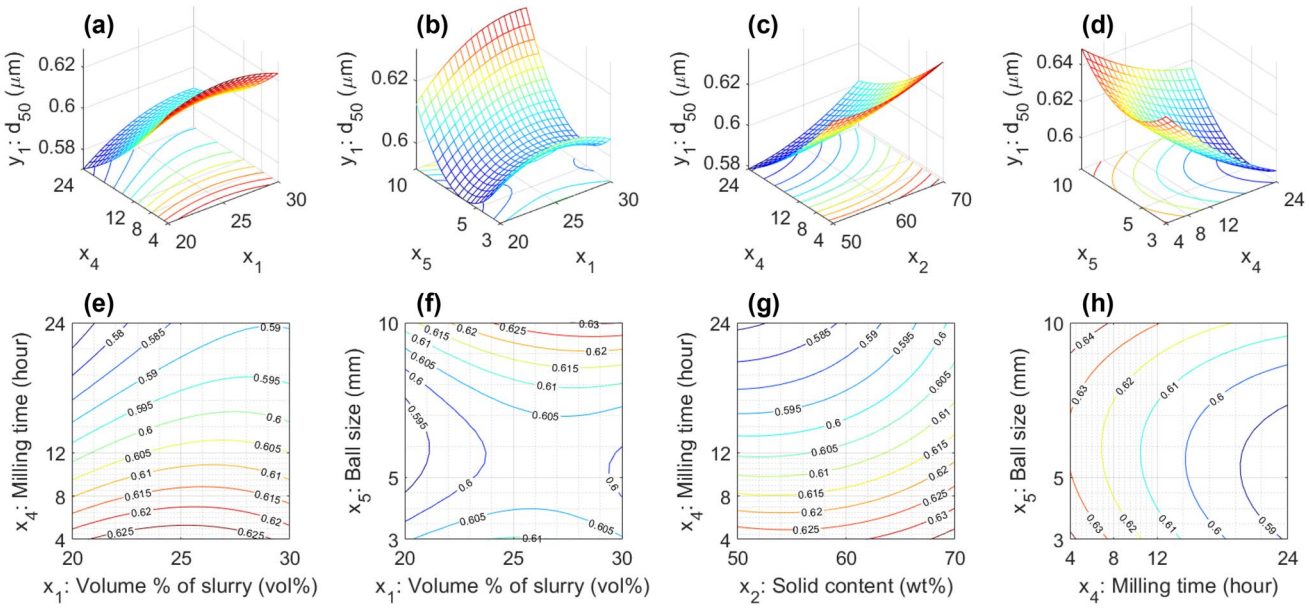

Fig. 5 Response surface plots (**a**–**d**) and contour plots (**e**–**h**) for the reduced model in Eq. (8). For convenience of interpretations, the ranges of X and Y axes have been recovered from the range $[-1, 1]$ to their original ranges

is proper to set the order of polynomial to be equal to 2. To train the models, the "fitlm" MATLAB function in Statistics and Machine Learning Toolbox can be used.

After training the three full models, statistically significant terms can be identified by testing whether the p values are smaller than 0.1 or not. The reduced models can be obtained by eliminating all the remaining terms except for the statistically significant terms from the full models. The following regression functions can be derived by refitting the reduced models to the 180 data pairs:

$$\begin{aligned}\hat{y}_1(\mathbf{x}) = {} & \underset{(.0031)}{.6023} + \underset{(.0013)}{.0046}x_1 + \underset{(.0012)}{.0078}x_2 - \underset{(.0012)}{.0052}x_3 - \underset{(.0014)}{.0216}x_4 + \underset{(.0012)}{.0083}x_5 \\ & + \underset{(.0016)}{.0047}x_1x_4 + \underset{(.0014)}{.0040}x_1x_5 + \underset{(.0016)}{.0034}x_2x_4 + \underset{(.0016)}{.0048}x_4x_5 \\ & - \underset{(.0023)}{.0056}x_1^2 + \underset{(.0023)}{.0043}x_2^2 + \underset{(.0024)}{.0051}x_4^2 + \underset{(.0026)}{.0164}x_5^2 \end{aligned} \tag{8}$$

$$\begin{aligned}\hat{y}_2(\mathbf{x}) = {} & \underset{(.027)}{1.725} + \underset{(.012)}{.076}x_1 + \underset{(.012)}{.040}x_2 + \underset{(.012)}{.031}x_3 - \underset{(.014)}{.188}x_4 + \underset{(.012)}{.174}x_5 \\ & - \underset{(.014)}{.024}x_2x_3 + \underset{(.015)}{.060}x_3x_5 + \underset{(.025)}{.076}x_4^2 - \underset{(.027)}{.245}x_5^2 \end{aligned} \tag{9}$$

$$\begin{aligned}\hat{y}_3(\mathbf{x}) = {} & \underset{(.0048)}{.3245} + \underset{(.0019)}{.0149}x_1 + \underset{(.0019)}{.0097}x_2 - \underset{(.0021)}{.0420}x_4 + \underset{(.0018)}{.0419}x_5 \\ & + \underset{(.0022)}{.0110}x_1x_5 + \underset{(.0022)}{.0056}x_2x_5 + \underset{(.0022)}{.0038}x_3x_5 \\ & + \underset{(.0035)}{.0086}x_2^2 - \underset{(.0035)}{.0066}x_3^2 + \underset{(.0037)}{.0153}x_4^2 - \underset{(.0040)}{.0069}x_5^2 \end{aligned} \tag{10}$$

where the SEs of the estimated coefficients are presented in parentheses at the bottom of them. The regression models in Eqs. (8)–(10) will be extensively exploited as follows. First, for any setting values of processing parameters, the models can calculate the predicted values of quality responses and their prediction intervals. Second, based on the regression models, response surface and contour plots can be plotted to visually understand how the processing parameters affect quality responses. Third, the importance values of inputs for each output can be quantified by applying the MC-based method to the regression functions.

Table 2 lists performance indices such as root mean squared error (RMSE), R^2, adjusted R^2, and F-statistic of the full and reduced models. Since the number of coefficients to be estimated is decreased when reducing the complexity of the models, the degree of freedom for the error term ε_l ($l = 1,\ldots, 3$) is increased, and thus the RMSE values can be decreased. In the reduced models, the values of R^2 are smaller than those in the full models, but the values of adjusted R^2 are larger than or equal to those in the full models. This indicates that for the given dataset the generalization capabilities of the reduced models are better than the full models. In the case of F-statistic, its values have become larger after reducing the number of the coefficients, and thus it is valid to say that the reduced models are more statistically significant.

Figure 5 shows response surfaces and contour plots visualizing the input–output relationships of the reduced model $\hat{y}_1(\mathbf{x})$ in Eq. (8); as space is limited, those of $\hat{y}_2(\mathbf{x})$ and $\hat{y}_3(\mathbf{x})$ are not presented here. In Fig. 5, two variables at X and Y axes are relevant to the interaction terms in Eq. (8);. By examining these figures carefully, it is possible to qualitatively understand how the two variables interact with each

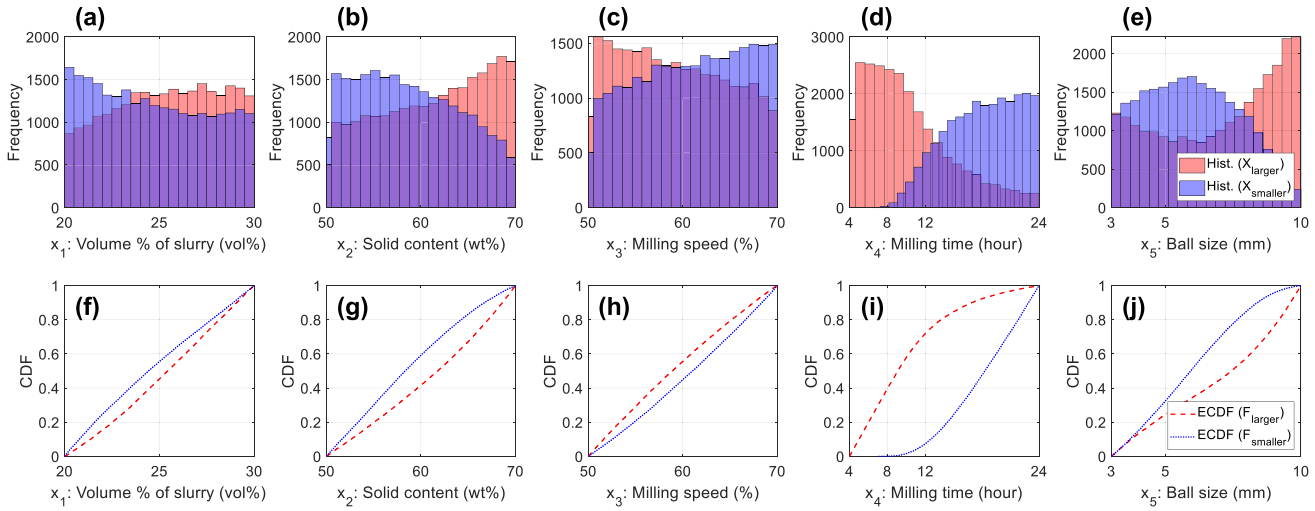

Fig. 6 Histograms of $x_1,\ldots, x_5$ associated with X^1_{larger} and X^1_{smaller}(**a**–**e**) and estimated ECDFs $F^1_{\text{larger}}(x_j)$ and $F^1_{\text{smaller}}(x_j)$, $j=1,\ldots, 5$ (f-j). In **a**–**e**, for convenience of interpretations, the ranges of X axes have been recovered from the range $[-1, 1]$ to their original ranges

other for the response. In Fig. 5e–h, as the width of contours become narrower, the change rates of quality responses become larger when we move in the orthogonal direction to contour lines. As shown in Fig. 5a and e, and Fig. 5c and g, in the early stages of milling (i.e., when $x_4 \leq 8$ h), the changes of x_1 and x_2 have little effect on y_1; when the value of x_4 is equal to 24 h, the value of y_1 tends to be proportional to the values of x_1 and x_2. It is also observed that reduction rate in y_1 deteriorates with increasing the values of x_1 and x_2. In Fig. 5b and f, it can be seen that as the value of x_5 becomes larger, the change of x_1 has more effect on the value of y_1. Figures 5d and h show that the longer the milling time, the larger the performance differences with respect to the d_{50} between 3 and 10 mm balls.

To estimate the importance values of the five inputs, $N=50{,}000$ uniform random vectors $\mathbf{x}^{(i)} \sim \mathbf{U}[-1, 1]^5$ are generated and substituted into Eqs. (8)–(10). Figure 6a–e show the histograms of $x_1,\ldots, x_5$ associated with the two sets X^1_{larger} and X^1_{smaller}, and Fig. 6f–j describe the estimated ECDFs $F^1_{\text{larger}}(x_j)$ and $F^1_{\text{smaller}}(x_j)$, $j=1,\ldots, 5$; the histograms and the estimated ECDFs relevant to $l=2$ and 3 are omitted due to space constraints. Figure 7 depicts bar graphs illustrating the importance values of $x_1,\ldots, x_5$ for $y_1,\ldots, y_3$ estimated based on the ECDFs in Fig. 6f–j. As can be seen in Fig. 7a, x_4 is the most important parameter for changing the value of y_1, and followed in order by x_5, x_2, x_3, and x_1. Figure 7b and c indicate that x_4, x_5, and x_1 make the first, second, and third largest contributions in determining the values of y_2 and y_3; the importance values of x_2 and x_3 for y_2 are similar to each other, but x_2 is more important parameter for y_3 than x_3.

5.2 Results of optimization

After appointing proper desirability function $d_l(\bullet)$, $l=1,\ldots, 3$, to each of the functions in Eqs. (8)–(10)., an overall desirability function $D(\mathbf{x})$ used as an objective function can be defined by Eq. (5). Since some desired target values are set for the value of the d_{50} (y_1), Eq. (3) is employed for $d_1(\bullet)$; in general, width (y_2) and skewness (y_3) are required to be minimized, Eq. (4) is used for $d_2(\bullet)$ and $d_3(\bullet)$.

Table 3 lists the optimization results of applying the method in Fig. 2 for maximizing $D(\mathbf{x})$ when the following target values were set up for the three responses and the parameter value of x_5 was constrained to 3 mm: $y_{1,\text{target}}=0.58$ μm, $y_{2,\text{target}}=$ "min," and $y_{3,\text{target}}=$ "min." Here, the goal is to find the parameter points that can produce the following milled powder: its PSD is centered at the desired value of d_{50}, and at the same time, its width and both sides are as narrow and symmetrical as possible, respectively. The reason why the ball size (x_5) was restricted to be 3 mm is that it is a discrete input parameter, and thus its optimized values without the constrained condition cannot be used in practice. In Fig. 2, the values of α, K, and K' are set to 0.01, 100, and 10, respectively. In Table 3, the optimized parameter points and their model outputs are summarized in the second to sixth columns and the seventh to ninth columns, respectively; the 99% PIs enclosing the outputs are also presented at the bottom of the model outputs. As listed in the table, the outputs of $\mathbf{x}^*_{(1)}, \ldots, \mathbf{x}^*_{(10)}$ are the same or very similar to each other, but the optimized parameter values of x^*_2 and x^*_3 in $\mathbf{x}^*_{(1)}$ and $\mathbf{x}^*_{(2)}$ are quite different from those of others; this is due to the fact that since there are infinitely many input points

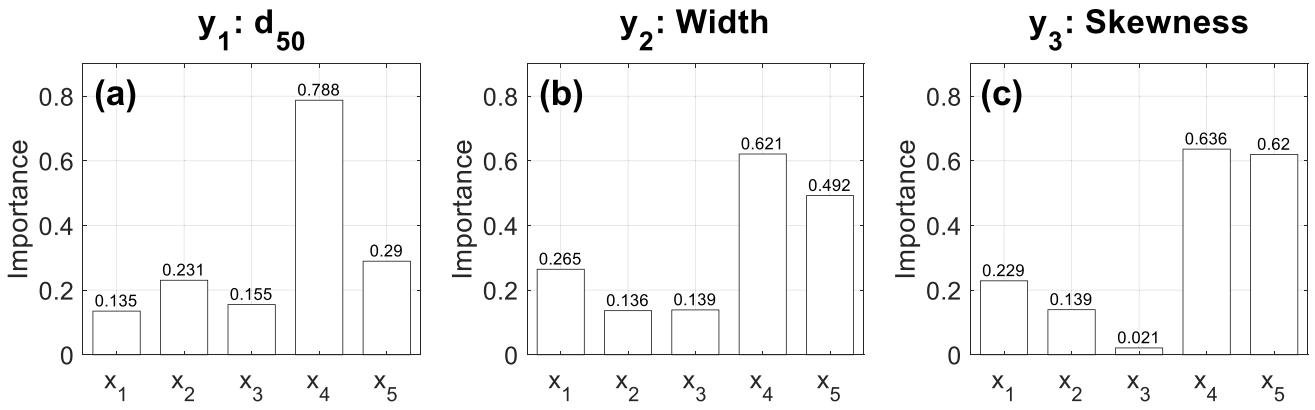

Fig. 7 Estimated importance values of $x_1,\ldots, x_5$ for **a** y_1: d_{50}, **b** y_2: width, and **c** y_3: skewness

that can achieve the target value $y_{1,\text{target}} = 0.58$ μm (see Fig. 5e), optimization algorithms cannot find a unique solution. The optimized parameter intervals by the method in Fig. 4 with $\alpha = 0.01$ are presented at the bottom of the parameter values in $\mathbf{x}^*_{(1)}$ and $\mathbf{x}^*_{(3)}$ marked with boldface; the upper and lower bound vectors $\mathbf{x}^*_{UB}$ and $\mathbf{x}^*_{LB}$ for $\mathbf{x}^*_{(1)}$ are $[23.55, 70.00, 70.00, 24.00, 4.70]^T$ and $[20.00, 55.09, 61.77, 19.12, 3.00]^T$, respectively. Figure 8 shows the contour plots of the regression function $\hat{y}_1(\mathbf{x})$ at which the first solution $\mathbf{x}^*_{(1)}$ and the input region defined by its optimized parameter intervals are indicated by red asterisks and dashed black lines, respectively. In these plots, it should be noted that the model outputs of the input vectors included in the input region are very close to $y_{1,\text{target}} = 0.58$ μm. This suggests that the optimized intervals allow to know the tolerable setting errors of each parameter, and depending on field situations, it is also possible to flexibly adjust its values within the region. Table 4 summarizes the results of applying the

Table 3 ($y_{1,\text{target}} = 0.58$ μm, $y_{2,\text{target}} =$ "min," $y_{3,\text{target}} =$ "min") Optimized parameter points by the method in Fig. 2 and their model outputs. The optimized parameter intervals by the method in Fig. 4 are presented at the bottom of the parameter values in $\mathbf{x}^*_{(1)}$ and $\mathbf{x}^*_{(3)}$

Order	Optimized parameter point $\mathbf{x}^*$					Model output		
	x_1^*	x_2^*	x_3^*	x_4^*	x_5^*	$\hat{y}_1(\mathbf{x}^*)$	$\hat{y}_2(\mathbf{x}^*)$	$\hat{y}_3(\mathbf{x}^*)$
1	**20.03**	**63.34**	**70.00**	**22.74**	**3.00**	**0.580**	**1.102**	**0.239**
	[20.00, 23.55]	**[55.09, 70.00]**	**[61.77, 70.00]**	**[19.12, 24.00]**	**[3.00, 4.70]**	**[0.544, 0.616]**	**[0.744, 1.460]**	**[0.184, 0.293]**
2	20.11	63.48	70.00	22.94	3.00	0.580	1.102	0.239
						[0.544, 0.616]	[0.744, 1.460]	[0.184, 0.293]
3	**20.01**	**52.83**	**50.00**	**23.04**	**3.00**	**0.580**	**1.106**	**0.245**
	[20.00, 23.42]	**[50.00, 60.83]**	**[50.00, 57.98]**	**[19.53, 24.00]**	**[3.00, 4.65]**	**[0.544, 0.616]**	**[0.746, 1.465]**	**[0.191, 0.300]**
4	20.00	52.81	50.00	23.01	3.00	0.580	1.106	0.245
						[0.544, 0.616]	[0.746, 1.465]	[0.191, 0.300]
5	20.00	52.75	50.00	23.00	3.00	0.580	1.105	0.245
						[0.544, 0.616]	[0.746, 1.465]	[0.191, 0.300]
6	20.00	52.58	50.00	22.97	3.00	0.580	1.104	0.245
						[0.544, 0.616]	[0.745, 1.464]	[0.191, 0.300]
7	20.00	52.58	50.00	22.97	3.00	0.580	1.104	0.245
						[0.544, 0.616]	[0.745, 1.464]	[0.191, 0.300]
8	20.00	52.55	50.00	22.97	3.00	0.580	1.104	0.245
						[0.544, 0.616]	[0.745, 1.464]	[0.191, 0.300]
9	20.00	52.54	50.00	22.96	3.00	0.580	1.104	0.245
						[0.544, 0.616]	[0.745, 1.464]	[0.191, 0.300]
10	20.00	52.43	50.00	22.95	3.00	0.580	1.103	0.246
						[0.544, 0.616]	[0.744, 1.463]	[0.191, 0.300]

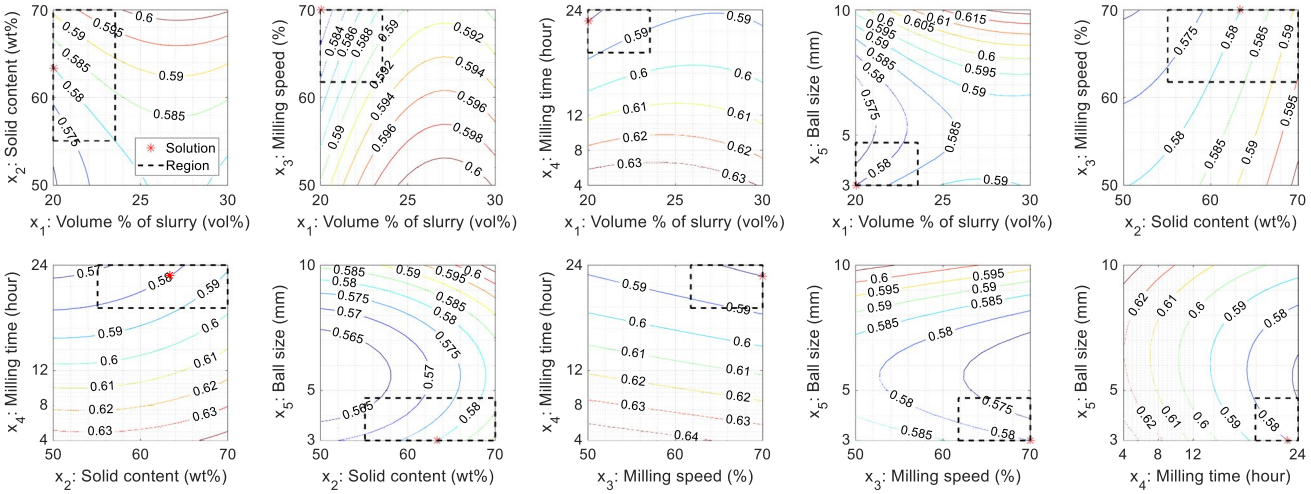

Fig. 8 Contour plots of $\hat{y}_1(\mathbf{x})$ with $\mathbf{x}^*_{(1)}$ in Table 3 and the input region defined by its optimized parameter intervals. For convenience of interpretations, the ranges of X and Y axes have been recovered from the range [− 1, 1] to their original ranges

method in Fig. 2 to the optimization problem with the target values $y_{1,\text{target}} = 0.60$ μm, $y_{2,\text{target}} =$ "min," and $y_{3,\text{target}} =$ "min," and with the equality constraint $x_5 = 3$ mm. As presented in the table, although the values of x_2^* and x_4^* in $\mathbf{x}^*_{(9)}$ are markedly different from those in others, all the outputs are the same or quite similar. The parameter intervals optimized by the method in Fig. 4 are indicated at the bottom of the parameter values in $\mathbf{x}^*_{(1)}$ and $\mathbf{x}^*_{(9)}$.

The productivity of the target mill is directly related with such input parameters as solid content (x_2), milling speed (x_3), and milling time (x_4) [55]. The solid content determines the amount of produced final powders, and

Table 4 ($y_{1,\text{target}} = 0.60$ μm, $y_{2,\text{target}} =$ "min," $y_{3,\text{target}} =$ "min") Optimized parameter points by the method in Fig. 2 and their model outputs. The optimized parameter intervals by the method in Fig. 4 are presented at the bottom of the parameter values in $\mathbf{x}^*_{(1)}$ and $\mathbf{x}^*_{(9)}$

Order	Optimized parameter point $\mathbf{x}^*$					Model output		
	x_1^*	x_2^*	x_3^*	x_4^*	x_5^*	$\hat{y}_1(\mathbf{x}^*)$	$\hat{y}_2(\mathbf{x}^*)$	$\hat{y}_3(\mathbf{x}^*)$
1	**22.00**	**63.40**	**50.00**	**20.67**	**3.00**	**0.600**	**1.219**	**0.252**
	[20.00, 26.39]	**[53.04, 70.00]**	**[50.00, 60.26]**	**[16.00, 24.00]**	**[3.00, 5.00]**	**[0.565, 0.635]**	**[0.863, 1.576]**	**[0.198, 0.306]**
2	21.83	64.15	50.00	20.98	3.00	0.600	1.219	0.252
						[0.565, 0.635]	[0.862, 1.576]	[0.198, 0.306]
3	21.73	63.75	50.00	20.62	3.00	0.600	1.218	0.252
						[0.565, 0.635]	[0.861, 1.575]	[0.198, 0.306]
4	21.70	63.83	50.00	20.63	3.00	0.600	1.218	0.252
						[0.565, 0.635]	[0.861, 1.575]	[0.198, 0.306]
5	21.79	64.35	50.01	21.06	3.00	0.600	1.219	0.252
						[0.565, 0.635]	[0.862, 1.576]	[0.198, 0.306]
6	21.79	64.47	50.00	21.15	3.00	0.600	1.219	0.252
						[0.565, 0.635]	[0.862, 1.576]	[0.198, 0.306]
7	21.63	62.90	50.00	20.02	3.00	0.600	1.217	0.252
						[0.565, 0.635]	[0.860, 1.574]	[0.198, 0.307]
8	21.58	63.59	50.00	20.36	3.00	0.600	1.217	0.252
						[0.565, 0.635]	[0.860, 1.574]	[0.198, 0.307]
9	**21.62**	**54.07**	**50.00**	**17.20**	**3.00**	**0.600**	**1.193**	**0.259**
	[20.00, 24.70]	**[50.00, 61.32]**	**[50.00, 57.18]**	**[13.93, 20.46]**	**[3.00, 4.45]**	**[0.565, 0.635]**	**[0.835, 1.552]**	**[0.205, 0.313]**
10	21.53	63.82	50.00	20.45	3.00	0.600	1.217	0.252
						[0.565, 0.635]	[0.860, 1.574]	[0.198, 0.307]

Table 5 Measured quality responses from four milled powders by $\mathbf{x}^*_{(1)}$ in Table 3

Index	y_1: d_{50}	y_2: width	y_3: skewness
1	0.603	0.937	0.207
2	0.604	1.031	0.226
3	0.587	1.044	0.237
4	0.581	0.957	0.219
Average	0.594	0.992	0.222

Table 6 Measured quality responses from four milled powders by $\mathbf{x}^*_{(3)}$ in Table 3

Index	y_1: d_{50}	y_2: width	y_3: skewness
1	0.567	0.951	0.217
2	0.589	1.054	0.237
3	0.593	1.042	0.230
4	0.588	1.060	0.239
Average	0.584	1.027	0.231

milling speed and time are relevant to the amount of electrical energy consumption (i.e., production costs). Among the $K' = 10$ solutions listed in Tables 3 and 4, process operators and engineers can select and use appropriate solutions in consideration of the productivity. In Table 3, to satisfy the target values, and at the same time to produce the larger amount of milled powders,$\mathbf{x}^*_{(1)}$ or $\mathbf{x}^*_{(2)}$ with higher value of x_2 can be used. The values of x_2 in $\mathbf{x}^*_{(1)}$ and $\mathbf{x}^*_{(2)}$ are about 10 wt% higher than those of others, but all the values of x_1 and x_4 in Table 3 are extremely similar to each other. However, if $\mathbf{x}^*_{(1)}$ or $\mathbf{x}^*_{(2)}$ is used, the container should be rotated with higher milling speed (i.e.,$x^*_3 = 70\%$), and thus the amount of the energy consumption increases. In Table 4, to attain the target values and to reduce production time simultaneously,$\mathbf{x}^*_{(9)}$ can be used; it can save the time by 3.47 h compared to $\mathbf{x}^*_{(1)}$. However, the value of x_2 in $\mathbf{x}^*_{(9)}$ is 9.33 wt% lower than that in $\mathbf{x}^*_{(1)}$, and thus the amount of produced powders by $\mathbf{x}^*_{(9)}$ will be smaller than $\mathbf{x}^*_{(1)}$.

5.3 Results of confirmation experiments

To verify the effectiveness of the optimized parameter points, confirmation experiments were performed based on $\mathbf{x}^*_{(1)}$ and $\mathbf{x}^*_{(3)}$ in Table 3, and $\mathbf{x}^*_{(1)}$ and $\mathbf{x}^*_{(9)}$ in Table 4. In these experiments, the milling parameters were set up in accordance with the optimized points, the final powders were produced, and then their three quality responses were measured. Considering the process uncertainties, the same experiments were repeated four times for each of the above four optimized parameter points.

Tables 5 and 6 list the measured quality responses from the four milled powders produced by the optimized points $\mathbf{x}^*_{(1)}$ and $\mathbf{x}^*_{(3)}$ in Table 3, respectively; the averaged values of the measured responses are also summarized at the last row in each table. In these tables, the indices 1, 2, 3, and 4 correspond to the four repeated experiments, respectively. Figure 9a and b show the PSDs of the four milled powders in Tables 5 and 6, respectively. In Table 5, the measured values of d_{50} from the 1st and 2nd powders are 0.603 μm and 0.604 μm, approximately 0.02 μm higher than its target value (i.e., 0.58 μm); their measured values of y_2 and y_3 are smaller than the model outputs $\hat{y}_2(\mathbf{x}^*_{(1)}) = 1.102$ and $\hat{y}_3(\mathbf{x}^*_{(1)}) = 0.239$, respectively. The measured values of d_{50} from 3rd and 4th powders are similar with its target value and their values of y_2 and y_3 are also smaller than the model outputs. In Table 6, the differences between all the measured values of y_1 and its target value are less than or equal to 0.013 μm, and the smaller values of y_2 and y_3 than the outputs $\hat{y}_2(\mathbf{x}^*_{(3)}) = 1.106$ and $\hat{y}_3(\mathbf{x}^*_{(3)}) = 0.245$ have been obtained. Since all the measured responses in Tables 5 and 6 belong to the PIs in Table 3, it can be understood that the procedure in Fig. 1 can achieve the statistically reliable optimization results. The average values of the responses in Tables 5 and 6 differ in the d_{50}, width, and skewness by 0.01 μm, 0.035, and 0.009, respectively; since $\mathbf{x}^*_{(1)}$ and $\mathbf{x}^*_{(3)}$ get the similar measured responses to each other, it seems reasonable to suppose that either one can be used to produce the final powder satisfied with the target values.

Tables 7 and 8 summarize the measured responses of the four powders obtained by $\mathbf{x}^*_{(1)}$ and $\mathbf{x}^*_{(9)}$ in Table 4, respectively. It can be confirmed that all the responses are included in the PIs in Table 4. The differences in the averaged values of d_{50}, width, and skewness between Tables 7 and 8 are 0.008, 0.007, and 0.003, respectively; these are negligible taking the process uncertainties into account. Figure 10a and b present the PSDs relevant to the four powders in Tables 7 and 8, respectively. As can be viewed from these figures, the four PSDs measured by the four repeated experiments are extremely similar in shape; the

Table 7 Measured quality responses from four milled powders by $\mathbf{x}^*_{(1)}$ in Table 4

Index	y_1: d_{50}	y_2: width	y_3: skewness
1	0.623	1.077	0.243
2	0.632	1.066	0.240
3	0.611	1.098	0.249
4	0.615	1.085	0.244
Average	0.620	1.082	0.244

Table 8 Measured quality responses from four milled powders by $\mathbf{x}^*_{(9)}$ in Table 4

Index	y_1: d_{50}	y_2: width	y_3: skewness
1	0.611	1.079	0.241
2	0.610	1.080	0.244
3	0.611	1.097	0.251
4	0.616	1.099	0.253
Average	0.612	1.089	0.247

shape of PSDs shown in each of Fig. 10a and b are also quite similar to each other.

6 Conclusions

In this study, ML approach based on polynomial regression models was introduced to quantitatively analyze the optimal processing parameters and predict the target particle sizes for ball milling of alumina ceramics. Median particle size, width, and skewness of PSDs for milled powders were regarded as quality responses. The volume percent of slurry, solid content, milling speed, milling time, and ball size were considered as key input parameters to be optimized. PI-based point and interval optimization methods using polynomial regression analysis were proposed here. After deriving the functional relations between the inputs and the responses, and defining objective functions for solving MRO problems by desirability approach, the proposed methods were used to optimize both parameter points and intervals for accomplishing user-specified target responses.

The main advantages of the proposed PI-based parameter point and interval optimization methods in Figs. 2 and 4 can be emphasized as follows. First, most of previous studies for solving MRO problems did not provide a way to address the situation in which desired target values are established on some quality responses so that there is no unique solution. This paper proposes the PI-based point optimization method in Fig. 2 that can quantify the quality of different candidate solutions for the MRO problems according to their lengths of PIs and then can recommend statistically reliable solutions. Second, the previous studies focused mainly on optimizing parameter points and showed little concern for their interval optimization. This paper proposes the PI-based interval optimization method

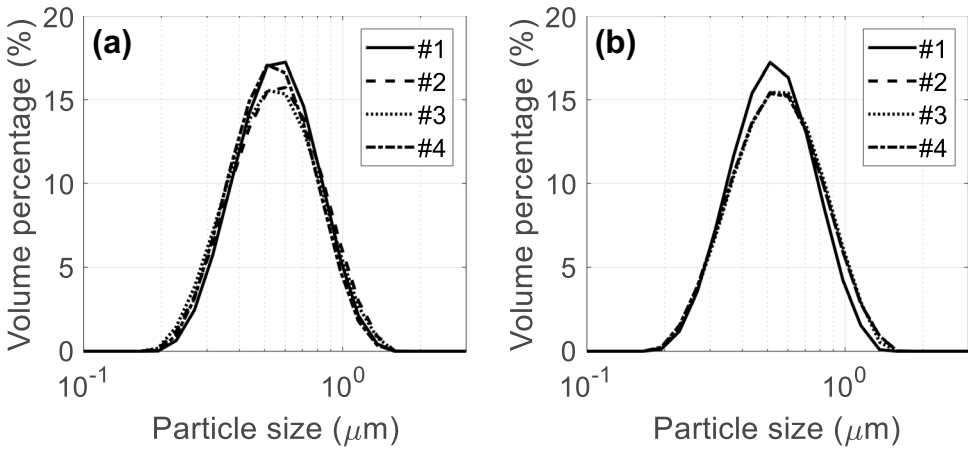

Fig. 9 PSDs of four milled powders in Tables 5 (**a**) and 6 (**b**) (#1, #2, #3, and #4 indicate the four different experiments)

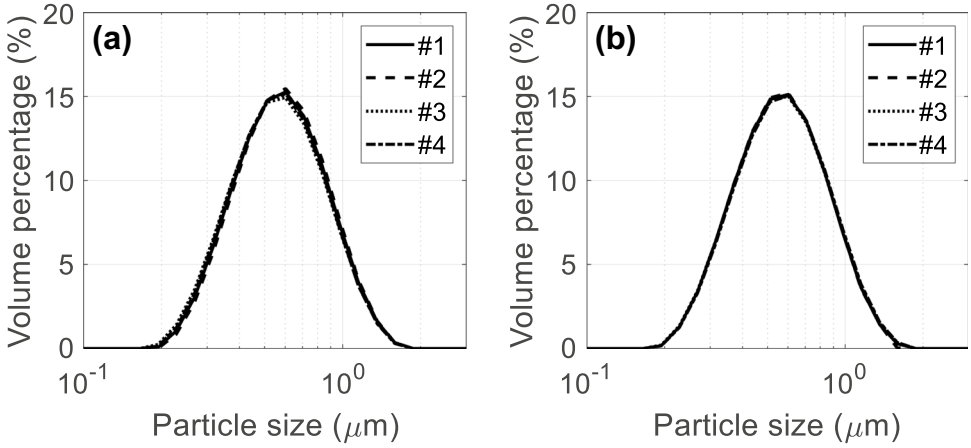

Fig. 10 PSDs of four milled powders in Tables 7 (**a**) and 8 (**b**) (#1, #2, #3, and #4 indicate the four different experiments)

in Fig. 4 that can optimize parameter intervals enclosing the optimized parameter points in the light of process uncertainties. The optimized intervals can help to assess tolerable setting errors of processing parameters and to fine-tune the optimized points within the input domain restricted by the intervals.

The optimization results showed that the proposed point optimization method can select and recommend statistically reliable optimized parameter points even though unique solutions for the objective functions do not exist. These results are established by additional confirmation experiments. Compared with the PSDs of starting powders with the tails skewed to the right side, those of final powders showed more symmetrical shapes; in addition, the final powders have the similar values of d_{50} to target values. Finally, although this study emphasized on the ball milling of alumina ceramics, the new approach reported herein could be applicable for other ceramic materials.

Nomenclature

L: Number of quality responses (inputs); p: Number of processing parameters (outputs); y_l, x_j: lTh output, and jth input; $\hat{y}_l(\mathbf{x})$: Regression function for lth output y_l; $\hat{y}_l(\mathbf{x}_{\text{new}})$: Output of lth regression function for new input vector x_{new}; $[PI^l_{LB}(\mathbf{x}_{\text{new}}), PI^l_{UB}(\mathbf{x}_{\text{new}})]$: Prediction interval for $\hat{y}_l(\mathbf{x}_{\text{new}})$; PI^l_k: Length of prediction interval $[PI^l_{LB}(\mathbf{x}^*_k), PI^l_{UB}(\mathbf{x}^*_k)]$; PI_k: Total length of L prediction intervals obtained by summing all the standardized values of $PI^1_k, ..., PI^L_k$; $\mathbf{I}_{\text{imp.}} \in \Re^{L\times p}$: Importance matrix that consists of importance values of p inputs for L outputs; $d_l(\bullet)$: Desirability function for lth output y_l; $y_{l,\text{target}}$: Target value for lth output y_l; $y_{l,\min}$, $y_{l,\max}$: Lower and upper limits of lth output y_l; $D(\mathbf{x})$: Overall desirability function (objective function for multiple response optimization problem); $\mathbf{x}^* = [x^*_1, ..., x^*_p]^T$: Optimized parameter point; $\mathbf{x}^*_{LB}, \mathbf{x}^*_{UB}$: Lower and upper bounds for defining optimized parameter intervals; $[x^*_{LB,j}, x^*_{UB,j}]$: Optimized parameter interval for jth input; $\mathbf{J}_{L\times p}$: L By p matrix of ones; δ_l: Small positive increment; W_{lj}, $\overline{W}_{lj}$: (l, j)Th element of $\mathbf{W} = \mathbf{J}_{L\times p} - \mathbf{I}_{\text{imp.}}$, and standardized values of W_{lj}; $\times^p_{j=1}[x^*_j - \delta_l \overline{W}_{lj}, x^*_j + \delta_l \overline{W}_{lj}]$: p-Dimensional hyper-rectangle centered at $\mathbf{x}^*$; $\mathbf{v}_m$, V: Vertices of hyper-rectangle, and vertex set composed of all $\mathbf{v}_m$

Abbreviations

ML: Machine learning; *PI*: Prediction interval; *ANN*: Artificial neural networks; *PSD*: Particle size distribution; *RSM*: Response surface method; *GA*: Genetic algorithm; *AVOVA*: Analysis of variance; *CCD*: Central composite design; *MRO*: Multiple response optimization; *MC*: Monte Carlo; *PSO*: Particle swarm optimization; *RMSE*: Root mean squared error; *ECDF*: Empirical cumulative distribution function

Supplementary Information The online version contains supplementary material available at https://doi.org/10.1007/s00170-022-10430-w.

Funding This work was supported by the Ministry of Trade, Industry and Energy (MOTIE) and the Korea Evaluation Institute of Industrial Technology (KEIT) research funding (Grant No. 20003891), and in part by Electronics and Telecommunications Research Institute (ETRI) grant funded by the Korean government [22ZD1120, Regional Industry ICT Convergence Technology Advancement and Support Project in Daegu-Gyeongbuk].

Data availability All data generated or mentioned in this study are included in this published article.

Code availability No code was provided in this manuscript.

Declarations

Ethics approval This study does not involve ethical issues.

Consent to participate All authors agreed to participate in this research.

Consent for publication All authors have reviewed the final version of manuscript and approve it for publication.

Conflict of interest The authors declare no competing interests.

References

1. Schmidt J, Marques MRG, Botti S, Marques MAL (2019) Recent advances and applications of machine learning in solid-state materials science. NPJ Comput Mater 5:83
2. Yang K, Xu X, Yang B, Cook B, Ramos H, Krishnan NMA, Smedskjaer MM, Hoover C, Bauchy M (2019) Predicting the Young's modulus of silicate glasses using high-throughput molecular dynamics simulations and machine learning. Sci Rep 9:8739
3. Liu H, Zhang T, Krishnan NMA, Smedskjaer MM, Ryan JV, Gin S, Bauchy M (2019) Predicting the dissolution kinetics of silicate glasses by topology-informed machine learning. NPJ Mater Degrad 3:32
4. Wei J, Chu X, Sun X-Y, Xu K, Deng H-X, Chen J, Wei Z, Lei M (2019) Machine learning in materials science. Infomat 1:338–358
5. Liu H, Fu Z, Yang K, Xu X, Bauchy M (2021) Machine learning for glass science and engineering: a review. J Non-Cryst Solids 557:119419
6. Yang H, Zhang Z, Zhang J, Zeng XC (2018) Machine learning and artificial neural network prediction of interfacial thermal resistance between graphene and hexagonal boron nitride. Nanoscale 10:19092
7. He J, Li J, Liu C, Wang C, Zhang Y, Wen C, Xue D, Cao J, Su Y, Qiao L, Bai Y (2021) Machine learning identified materials descriptors for ferroelectricity. Acta Mater 209:116815
8. Kerner J, Dogan A, Recum HV (2021) Machine learning and big data provide crucial insight for future biomaterials discovery and research. Acta Biomater 130:54–65

9. Rodrigues JF Jr, Florea L, de Oliveira MCF, Diamond D, Oliveira ON Jr (2021) Big data and machine learning for materials science. Discov Mater 1:12
10. Liu Y, Niu C, Wang Z, Gan Y, Zhu Y, Sun S, Shen T (2020) Machine learning in materials genome initiative: a review. J Mater Sci Technol 57:113–122
11. Kaufmann K, Maryanovsky D, Mellor WM, Zhu C, Rosengarten AS, Harrington TJ, Oses C, Toher C, Curtarolo S, Vecchio KS (2020) Discovery of high-entropy ceramics via machine learning. Npj Comput Mater 6:42
12. Kaufmann K, Vecchio KS (2020) Searching for high entropy alloys: a machine learning approach. Acta Mater 198:178–222
13. Qin J, Liu Z, Ma M, Li Y (2021) Machine learning approaches for permittivity prediction and rational design of microwave dielectric ceramics. J Materiomics 7:1284–1293
14. Qu N, Liu Y, Liao M, Lai Z, Zhou F, Cui P, Han T, Yang D, Zhu J (2019) Ultra-high temperature ceramics melting temperature prediction via machine learning. Ceram Int 45:18551–18555
15. Yang P, Wu S, Wu H, Lu D, Zou W, Chu L, Shao Y, Wu S (2021) Prediction of bending strength of Si_3N_4 using machine learning. Ceram Int 47:23919–23926
16. Reed JS (1995) Principles of ceramics processing, 2nd edn. Wiley, New York
17. Suryanarayana C (2001) Mechanical alloying and milling. Prog Mater Sci 46:1–184
18. Janot R, Guérard D (2005) Ball-milling in liquid media: applications to the preparation of anodic materials for lithium-ion batteries. Prog Mater Sci 50:1–92
19. Frances C, Laguerie C (1998) Fine wet grinding of an alumina hydrate in a ball mill. Powder Technol 99:147–153
20. Shin H, Lee S, Jung HS, Kim JB (2013) Effect of ball size and powder loading on the milling efficiency of a laboratory-scale wet ball mill. Ceram Int 39:8963–8968
21. Mulenga FK, Moys MH (2014) Effects of slurry pool volume on milling efficiency. Powder Technol 256:428–435
22. Wagih A, Fathy A, Kabeel AM (2018) Optimum milling parameters for production of highly uniform metal-matrix nanocomposites with improved mechanical properties. Adv Powder Technol 29:2527–2537
23. Oh HM, Park YJ, Kim HN, Ko JW, Lee HK (2021) Effect of milling ball size on the densification and optical properties of transparent Y_2O_3 ceramics. Ceram Int 47:4681–4687
24. Hou TH, Su CH, Liu WL (2007) Parameters optimization of a nanoparticle wet milling process using the Taguchi method, response surface method and genetic algorithm. Powder Technol 173:153–162
25. Zhang FL, Zhu M, Wang CY (2008) Parameters optimization in the planetary ball milling of nanostructured tungsten carbide/cobalt powder. Int J Refract Met Hard Mat 26:329–333
26. Ma J, Zhu SG, Wu CX, Zhang ML (2009) Application of back-propagation neural network technique to high-energy planetary ball milling process for synthesizing nanocomposite WC-MgO powders. Mater Des 30:2867–2874
27. Charkhi A, Kazemian H, Kazemeini M (2010) Optimized experimental design for natural clinoptilolite zeolite ball milling to produce nano powders. Powder Technol 203:389–396
28. Toraman OY, Katırcıoglu D (2011) A study on the effect of process parameters in stirred ball mill. Adv Powder Technol 22:26–30
29. Celep O, Aslan N, Alp İ, Taşdemir G (2011) Optimization of some parameters of stirred mill for ultra-fine grinding of refractory Au/Ag ores. Powder Technol 208:121–127
30. Ebadnejad A, Karimi GR, Dehghani H (2013) Application of response surface methodology for modeling of ball mills in copper sulphide ore grinding. Powder Technol 245:292–296
31. Canakci A, Erdemir F, Varol T, Patir A (2013) Determining the effect of process parameters on particle size in mechanical milling using the Taguchi method: measurement and analysis. Measurement 46:3532–3540
32. Patil AG, Anandhan S (2015) Influence of planetary ball milling parameters on the mechano-chemical activation of fly ash. Powder Technol 281:151–158
33. Erdemir F (2017) Study on particle size and X-ray peak area ratios in high energy ball milling and optimization of the milling parameters using response surface method. Measurement 112:53–60
34. Petrović S, Rožić L, Jović V, Stojadinović S, Grbić B, Radić N, Lamovec J, Vasilić R (2018) Optimization of a nanoparticle ball milling process parameters using the response surface method. Adv Powder Technol 29:2129–2139
35. Hajji H, Nasr S, Millot N, Salem EB (2019) Study of the effect of milling parameters on mechanosynthesis of hydroxyfluorapatite using the Taguchi method. Powder Technol 356:566–580
36. Santosh T, Rahul KS, Eswaraiah C, Rao DS, Venugopal R (2020) Optimization of stirred mill parameters for fine grinding of PGE bearing chromite ore, Particul. Sci Technol 9:1–13
37. Wu J, Jin S-H, Raju K, Lee Y, Lee H-K (2021) Analysis of individual and interaction effects of processing parameters on wet grinding performance in ball milling of alumina ceramics using statistical methods. Ceram Int 47:31202–31213
38. Draper NR, Smith H (1998) Applied regression analysis, 3rd edn. John Wiley & Sons Inc, New York
39. Montgomery DC, Peck EA, Vining GG (2012) Introduction to linear regression analysis, 5th edn. Wiley, New Jersey
40. Aggarwal A, Singh H, Kumar P, Singh M (2008) Optimizing power consumption for CNC turned parts using response surface methodology and Taguchi's technique-a comparative analysis. J Mater Process Technol 200:373–384
41. Costa N, Garcia J (2016) Using a multiple response optimization approach to optimize the coefficient of performance. Appl Therm Eng 96:137–143
42. Mostafanezhad H, Menghari HG, Esmaeili S, Shirkharkolaee EM (2018) Optimization of two-point incremental forming process of AA1050 through response surface methodology. Measurement 127:21–28
43. Parida MK, Joardar H, Rout AK, Routaray I, Mishra BP (2019) Multiple response optimizations to improve performance and reduce emissions of Argemone Mexicana biodiesel-diesel blends in a VCR engine. Appl Therm Eng 148:1454–1466
44. Yaliwal VS, Banapurmath NR, Gaitonde VN, Malipatil MD (2019) Simultaneous optimization of multiple operating engine parameters of a biodiesel-producer gas operated compression ignition (CI) engine coupled with hydrogen using response surface methodology. Renew Energy 139:944–959
45. Deng B, Shi Y, Yu T, Kang C, Zhao P (2018) Multi-response parameter interval sensitivity and optimization for the composite tape winding process. Materials 11:220
46. Chen Z, Shi Y, Lin X, Yu T, Zhao P, Kang C, He X, Li H (2019) Analysis and optimization of process parameter intervals for surface quality in polishing Ti-6Al-4V blisk blade. Results Phys 12:870–877
47. Castillo ED (2007) Process optimization: a statistical approach. Springer Science & Business Media, LLC, New York
48. Candioti LV, De Zan MM, Cámara MS, Goicoechea HC (2014) Experimental design and multiple response optimization using the desirability function in analytical methods development. Talanta 124:123–138
49. Mohanty S, Mishra A, Nanda BK, Routara BC (2018) Multi-objective parametric optimization of nano powder mixed electrical discharge machining of $AlSiC_p$ using response surface methodology and particle swarm optimization. Alex Eng J 57:609–619

50. Yu J, Yang S, Kim J, Lee Y, Lim KT, Kim S, Ryu S-S, Jeong H (2020) A confidence interval-based process optimization method using second-order polynomial regression analysis. Processes 8:1206
51. Kennedy J, Eberhart R (1995) Particle swarm optimization. Proceedings of ICNN'95 - International Conference on Neural Networks 4:1942–1948
52. Engelbrecht AP (2007) Computational intelligence: an introduction, 2nd edn. John Wiley & Sons Ltd, England
53. Del Valle Y, Venayagamoorthy GK, Mohagheghi S, Hernandez JC, Harley RG (2008) Particle swarm optimization: basic concepts, variants and applications in power systems. IEEE Trans Evol Comput 12:171–195
54. Dayar T, Orhan MC (2016) Cartesian product partitioning of multidimensional reachable state spaces. Probab Eng Inform Sci 30:413–430
55. Razavi-Tousi SS, Szpunar JA (2015) Effect of ball size on steady state of aluminum powder and efficiency of impacts during milling. Powder Technol 284:149–158